Med Biol Eng Comput (2018) 56:695–707
DOI 10.1007/s11517-017-1717-8

ORIGINAL ARTICLE

# A monocentric centerline extraction method for ring-like blood vessels

**Fengjun Zhao[1] · Feifei Sun[1] · Yuqing Hou[1] · Yanrong Chen[1] · Dongmei Chen[2] · Xin Cao[1] · Huangjian Yi[1] · Bin Wang[1] · Xiaowei He[1] · Jimin Liang[3]**

Received: 11 March 2017 / Accepted: 17 August 2017 / Published online: 2 September 2017


**Abstract** Centerline is generally used to measure topological and morphological parameters of blood vessels, which is pivotal for the quantitative analysis of vascular diseases. However, previous centerline extraction methods have two drawbacks on complex blood vessels, represented as the failure on ring-like structures and the existing of multi-voxel width. In this paper, we propose a monocentric centerline extraction method for ring-like blood vessels, which consists of three components. First, multiple centerlines are generated from the seed points that are chosen by randomly sprinkling points on blood vessel data. Second, multi-centerline fusion is used to repair the notches of centerlines on ring-like vessels, and the local maximum of distance from oundary is employed to remedy the missing centerline points. Finally, monocentric processing is devised to keep the vascular centerline with single voxel width. We compared the proposed method with Wan et al.'s method and topological thinning on five groups of data including synthesized vascular datasets and MR brain images. The result showed the proposed method performed better than the two contrast methods both by visual inspection and by quantitative assessment, which demonstrated the performance of the proposed method on ring-like blood vessels as well as the elimination of multi-voxel width points.

**Keywords** Centerline extraction · Blood vessels · Information fusion · Monocentric processing

✉ Xiaowei He
hexw@nwu.edu.cn

✉ Jimin Liang
jimleung@mail.xidian.edu.cn

[1] School of Information Sciences and Technology, Northwest University, Xi'an, Shaanxi 710069, China

[2] College of Life Information Science and Instrument Engineering, Hangzhou Dianzi University, Hangzhou, Zhejiang 310018, China

[3] Engineering Research Center of Molecular and Neuro Imaging of Ministry of Education, School of Life Science and Technology, Xidian University, Xi'an, Shaanxi 710071, China

## 1 Introduction

Cardiovascular and cerebrovascular diseases are serious threats to human's health, which account for a majority of deaths in both the developed and the developing countries [24, 31]. Image analysis plays a significant role in the diagnosis and treatment of such diseases, among which centerline extraction is one of the most important components [9, 30]. The centerline is defined as the medial axis along a tubular blood vessel [12], commonly used in measuring the vascular topological and morphological parameters, such as vascular diameter, vascular length, vascular thickness, vascular junction, and segment tortuosity [42]. Therefore, centerline is a simplified morphological description of a blood vessel, with significant importance in the accurate location and quantitative analysis of cardiac-cerebral vascular diseases [15, 19, 35]. Besides, it can also be employed for fast registration of blood vessels and updating blood vessel models obtained intraoperatively [22, 23].

### 1.1 State-of-the-art methods

Nowadays, numerous scholars and researchers have studied and developed a plenty of centerline extraction methods, which can be roughly divided into two categories, i.e., the manual and automatic methods. The automatic centerline extraction methods have become the mainstream, which can be further divided into the following three categories.

**Shortest path algorithm** Dijkstra algorithm is a typical single-source shortest path algorithm for computing the shortest path from one node to all the other nodes and can be applied to create the distance map [17]. The main procedure of shortest path method is to grow a centerline from a starting point in the center until it reaches the end point. Without using the weight of distance from boundary (DFB-distance), the centerline always travels in the vicinity of corners especially on crooked objects [4, 26]. Wan et al. improved this method by bring the DFB-distance field into Dijkstra's shortest path algorithm. This method ensures that the centerline is located at the center of the tubular colon [36]. Li and Yezzi invented a four-dimensional (4D) minimal path method for centerline and vessel extraction [28]. They modeled each blood vessel as 4D curves, consisting of three spatial coordinates and an extra vascular diameter dimension. The centerline is traced by a single and global minimal path in this higher dimensional domain between user-supplied end points. Starting from a root voxel, Jin et al.'s method iteratively adds new branches to the skeleton. The new branches are those connecting the farthest quench voxels to the current skeleton, found by a minimum cost path [18]. Antiga et al. developed a software package named VMTK, which semi-automatically extracts centerline based on Voronoi diagrams [1]. Each centerline point in Voronoi diagram framework can be considered as the center of a maximal inscribed sphere. The limitation is that VMTK requires manually assignment of all the starting and end points, which is a huge challenge when dealing with complex blood vessels. Currently, most of shortest path algorithms can extract satisfying centerlines that are approximated to the real center of tubular objects. However, most of these methods are based on three-dimensional (3D) distance map, which generally leads to disconnection when extracting centerlines on ring-like blood vessels.

**Topological thinning** Topological thinning is a traditional method in centerline extraction and has been widely used in colon and artery examination [3, 6, 8, 25, 33, 36]. The principle of this method is to peel off vessels layer by layer until the middle layer is left [16]. Similarly, Krissian et al. obtained the centerline by gradually deleting the simple points whose removal does not change the topology of the vessel [20, 21]. Bian et al. used graph-theoretic analysis to get the centerline of airway. The method can be divided into two steps: first, delete the border voxels symmetrically using topological thinning; second, prune the extra branches using graph-theoretic analysis [3]. Yang et al. obtained the skeleton of coronary artery by continuously eroding the boundary voxels after the removing the non-vessel structures with the improved Frangi's vesselness filter [39]. However, the speed is quite slow due to the mechanism limitation of topological thinning. Many researchers have devoted themselves to the issue of how to accelerate the topological thinning algorithm. For example, Arcelli et al. proposed a procedure that speeds up the thinning transformation and gets a well-shaped skeleton [6]. Sadleir et al. tried to improve the efficiency of the method by using lookup tables to reduce the computational cost of the thinning process [33]. Moreover, Lee et al. suggested a parallel thinning algorithm to extract both the centerline and the medial surfaces of 3D objects. By preserving the topological and the geometrical conditions, their algorithm produces desirable centerlines and performs well in terms of noise sensitivity and speed [27]. We refer the readers to [25] for a more comprehensive survey of thinning methodologies.

**Intensity-based method** There are also some centerline extraction methods based on the Hessian matrix, level sets, and so on. We define these methods as intensity-based methods, because all of them mainly exploit the intensity information of blood vessel images. Kumar et al. employed two dimensional cross section analysis to extract the centerline, where the vessel on the cross section image is found based on Hessian matrix, and then the central voxel of each cross section are connected to form the centerline [23]. Aylward et al. adopted the intensity ridge method to the problem of centerline extraction. This method represents an $N$-dimensional image as a surface in an $(N + 1)$-dimensional space by mapping the intensity to the height dimension, where the centerlines of tubular object will be represented as a one-dimensional height ridges on the surface [2, 32]. The limitation of this method lies in its sensitivity to initialization and noise. Based on region growing and level sets, Xu et al. gained the centerline of tree-like blood vessel by tracking the points of the largest curvature on the surface of the wave-front propagating from a point of skeleton line with level sets [38]. This method can effectively filter the noise interference. Furthermore, Matamoros et al. utilized the difference of offset Gaussians filters and region growing to extract the centerline. The points associated with the highest filter responses are detected as the candidates in four directions, followed by the collection of centerline segments via region growing process [29].

### 1.2 Problem and contribution

Most of previous methods perform well on the tree-like vascular networks and have been successfully applied in the clinical and preclinical quantitative analysis of vascular related diseases. Nevertheless, these methods have some drawbacks on the complex blood vessels, which are manifested in the following two aspects:

1. The shape of blood vessels varies, containing not only tree-like but also ring-like structures sometimes. The ring-like blood vessel is defined as a "head-tail" vessel structure, in which starting from any voxel on the ring-like

vessel one can return to this voxel along a certain direction. For example, the circle of Willis (CoW) (see Fig. 8) is a ring-like arterial blood vessel located at the bottom of the brain. It is the main arterial anastomoses in the brain and is responsible for the distribution of oxygenated blood throughout the cerebral mass [7, 37]. In this case, the centerline extracted by Wan et al.'s method in [36] is fractured and disconnected, because the seed and end points of the centerline on circular blood vessel are generally not fully connected with each other.

2. Multi-voxel width within extracted centerline often occurs in previous work, which is an obstacle to the accurate measurement of the parameters such as vascular length, vascular radius, vascular junction, and segment tortuosity [13, 14]. Thus, single voxel width is an important characteristic of the extracted centerline for the accurate computation of vascular parameters. It is also critical for the follow-up diagnosis and planning of vascular diseases. Unfortunately, few studies specially focus on this problem.

In this paper, we proposed a monocentric centerline extraction method for ring-like blood vessels. The proposed method repairs the incomplete centerline on ring-like blood vessels based on the multiple information fusion. Meanwhile, this method removes the unnecessary voxels using the monocentric processing of the centerline, to guarantee the centerline with single voxel width. The proposed method not only improves the continuity of the extracted centerline but also makes the centerline thinner, which is essential for the accurate computation of vascular parameters.

### 1.3 Structure of the paper

The structure of this paper is given as follows. We introduce the proposed centerline extraction method in Sect. 2, which consists of the recovery of incomplete centerline and the removal of centerline points with multi-voxel width. Results and performance evaluations are presented in Sect. 3. Finally, discussion and conclusions are given in Sects. 4 and 5 respectively.

## 2 Method

To solve the disconnection of circular centerline and multi-voxel width problem, we proposed a monocentric centerline extraction method for ring-like blood vessels. This method is based on binary blood vessels that have been segmented and can be decomposed into three components as shown in Fig. 1. First, we choose the seed points by sprinkling points randomly on the blood vessel data. The centerline is generated from the seed points based on the combination of distance from source (DFS-distance) and distance from boundary (DFB-distance) [36, 40]. Several original centerlines are obtained by different seed points. Second, we use multi-centerline fusion to repair the notches on the original centerlines and use local maximum of DFB-distance to correct the off-center points. Finally, monocentric processing of the centerline based on topological information is adopted to remove the redundant points on the centerline.

The rationale of our proposed method lies in the fusion of complementary information. The original centerlines provide the basic information about the true centerline. However, there are distortions in the notch positions on centerline for each ring-like blood vessel. Therefore, after retaining the correct information of all the original centerlines and modifying the distortions on notch positions, we readily obtain a theoretically accurate centerline on a ring-like blood vessel.

### 2.1 Acquisition of original centerline

We have mentioned above that Wan et al.'s method will lead to disconnection of centerline on ring-link blood vessel. The way centerline growing is starting from a seed point and tracking along the ring-like blood vessel, which generally does not guarantee the connection between the seed point and the end point. Thus, in this step, we first get the original centerlines with the notches (disconnection sites) locating at different positions, which will be used for the intact centerline extraction in Sect. 2.2.

For this goal, we improved Wan et al.'s method through sprinkling points with equal probability on the whole volumetric data (including both blood vessels and background), where the sprinkling is conducted by generating random number. The number of the sprinkled points is dependent on the size of the data, i.e., more points should be sprinkled on larger data to ensure enough points located at the volumetric data of blood vessels. The points falling on the blood vessel are treated as seed points. Then, centerlines are generated along the tubular blood vessel from the seed points by DFS-distance. The DFB-distance ensures that the voxels on the centerline are located at the center of blood vessel. The positions of the notches are various with different locations of the seed points. The first column of Figs. 1 and 2a shows the extracted centerlines with different notch positions.

### 2.2 Multiple information fusion

In this paper, we use the fusion of multiple information to solve the problem of centerline extraction on ring-like blood vessels, as illustrated in Fig. 2. In detail, we first use multi-centerline fusion to repair the notches on the original centerlines. Second, we adopt local maximum of DFB-distance to correct the off-center centerline points.

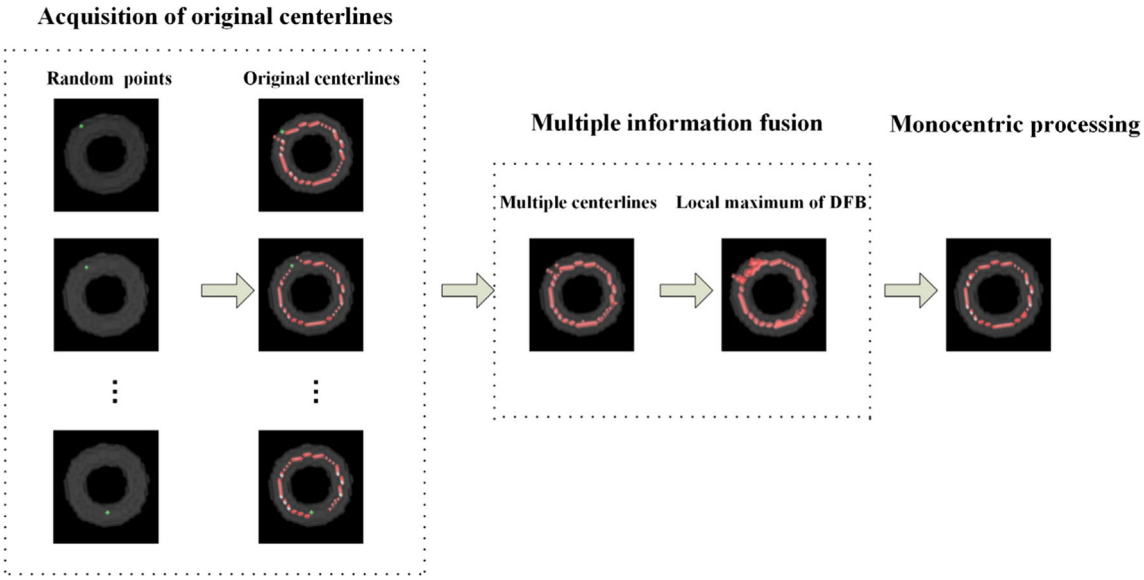


**Fig. 1** The framework of the proposed centerline extraction method

As we know, the locations of notches on the acquired original centerlines are different. If there are enough original centerlines, we are able to obtain a centerline that is correct and has no notches. If there is a notch on one centerline, meanwhile, there exists correctly distributed centerline points on the other centerlines at the same position. The overlapped information among these centerlines as complement can be exploited to form an intact centerline on the ring-like blood vessel (Fig. 2a, b). To utilize the complementary information, we merge the original centerlines together by the following equation.

$$C = C_1 \cup C_2 \cup \cdots \cup C_R \tag{1}$$

where $R$ is the number of original centerlines, $C_i$ is the $i$th original incomplete centerline, and $C$ is the centerline after combination. The more centerlines merged, the more valuable information can we obtain. But the errors accumulate simultaneously. Therefore, it is important to limit the number of merged centerline. Typically, two to three centerlines are enough for providing the complementary information.

We obtain most of the useful topological information of the objective centerline by multi-centerline fusion. However, there are off-center points after the centerline extraction, which means that some centerline points that should be on the centerline are missing (Fig. 2b). These missing centerline

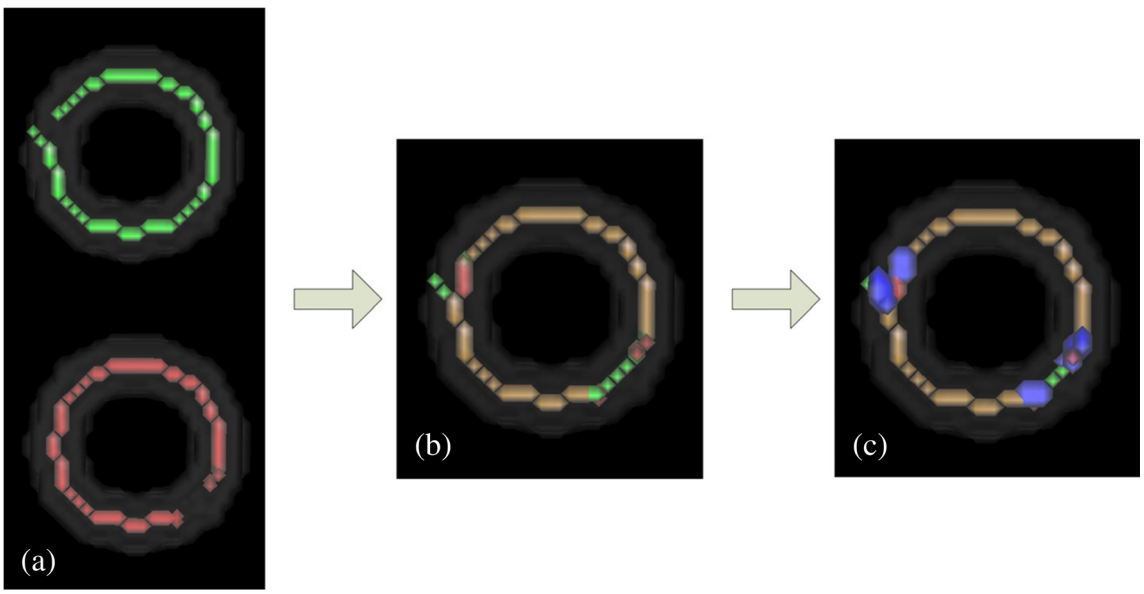


**Fig. 2** Diagram of multiple information fusion when using two original centerlines **a** Original centerlines. **b** Fusion of multiple centerlines. **c** Incorporation of neighbor points with larger DFB-distances

points are of great importance for the integrity and accuracy of the objective centerline.

To incorporate the missing centerline points, we first obtain the 26-neighbor of each centerline points on the merged centerline $C$. Second, we compare the DFB value of each centerline point with its 26-neighbor. If the DFB value for one of its 26-neighbors is larger than that of the centerline point, the neighbor is closer to the center and should be added into the merged centerline $C$ (Fig. 2c). In this case, we merge the neighbor point together with $C$ by using the following equation.

$$C^M = C \cup G \tag{2}$$

where $G$ is the set containing the missing centerline points (whose DFB values are larger than the centerline points), and $C^M$ is the centerline after the incorporation of local maximum of DFB-distance.

In this paper, we conduct the searching for neighbors of centerline point with larger DFB value only once. The rationale lies in that most of the cerebral blood vessels are approximated from 2 to 3 mm in diameter [34]. In general, the resolutions of CT or MRI images for human beings are no better than 500 μm [10]. This leads to the computed radii of the cerebral blood vessels are between two and three voxels. Thus, the comparison of DFB value among the centerline point and its neighbor only once is enough for finding the voxel with local maximum DFB value. If the vessel diameter is larger than 3 mm, the comparison can be conducted iteratively to extend the searching space.

### 2.3 Monocentric processing

Even though multiple information fusion repairs the notches of the centerline, it produces many redundant points which lead to the problem of multi-voxel width. Thus, it is necessary for us to singularize the centerline and remove the redundant centerline points with multi-voxel width.

There are two reasons for the existence of multi-voxel width on centerline. First, this phenomenon often occurs near the vascular branch or on the blood vessel whose radii change dramatically (Fig. 3a). Errors are easily induced in the vicinity of the vascular branch due to the high complexity of the vessel at this location. And the more branches exist at the same bifurcation, the more errors occur. Secondly, multi-centerline fusion can cause multi-voxel width on the extracted centerline (Fig. 3b). Moreover, the incorporation of voxels with local maximum of DFB-distances also produces multi-voxel width centerline.

In order to singularize the centerline, we adopt the monocentric processing to remove the points with multi-voxel width. Besides, we have to guarantee the connectivity of the extracted centerline after the removal of centerline points with multi-voxel width. Thus, which centerline points have the issue of multi-voxel width is critical for accurate monocentric processing. In this paper, the criterion is to judge if a set composed by current centerline point and its neighbors is within the set of another centerline point and its neighbors. If the answer is yes, we locate the current centerline point as the point with multi-voxel width and remove it subsequently. We give the detailed judgement and removal of centerline points with multi-voxel width as the following.

First of all, define $N$ as the number of neighbors of a centerline in terms of 26-neighborhood. $Nb(\cdot)$ is the neighboring operator. If $N > 2$, define $B = Nb(v)$ as the neighbor set of current centerline points $v$, and then $P_v = Nb(v) \cup \{v\}$ is a set containing current centerline point and its neighbors. For any one of the neighbors $b_i \in B$, $Q_{bi} = Nb(b_i) \cup \{b_i\}$ is a set containing one element $b_i$ and its neighbors. If $Q_{bi} \subset P_v$, all the neighbors of $b_i$ are within the region formed by the neighbors of $v$, which means that the centerline is still a connective region without $b_i$. Therefore, $b_i$ is a redundant centerline point and should be removed. If $Q_{bi} = P_v$, both the centerline point $v$ and $b_i$ are treated as the candidate points with multi-voxel width. In this case, which one should be removed is based on their DFB-distances. The higher the DFB value is, the closer is the point to the center. Thus, the point with smaller DFB value is redundant. If the DFB values of two candidate points are equal, the two points are equivalent and any one of them can be selected as the redundant point.

In order to illustrate the monocentric processing of the centerline clearly, we present an example as shown in Fig. 4. In Fig. 4a, $v$ is the current centerline point, with $B = Nb(v) = \{b_1, b_2, b_3\}$ and $P_v = Nb(v) \cup \{v\} = \{v, b_1, b_2, b_3\}$. The result of $Q_{bi}$ (where $i = 1, 2, 3$) is given as follows.

$$\begin{cases} Q_{b1} = Nb(b_1) \cup \{b_1\} = \{b_1, l, v\} \\ Q_{b2} = Nb(b_2) \cup \{b_2\} = \{b_2, b_3, v\} \\ Q_{b3} = Nb(b_3) \cup \{b_3\} = \{b_3, b_2, v, r\} \end{cases} \tag{3}$$

It is obvious that $Q_{b2} \subset P_v$. According to the criterion, voxel $b_2$ is a redundant centerline point and should be removed.

There is another circumstance when we select the candidate voxel as shown in Fig. 4b. In this case, we also select $v$ as the current centerline point with $B = Nb(v) = \{b_1, b_2, b_3\}$ and $P_v = Nb(v) \cup \{v\} = \{v, b_1, b_2, b_3\}$. The result of $Q_{bi}$ (where $i = 1, 2, 3$) is given as follows.

$$\begin{cases} Q_{b1} = Nb(b_1) \cup \{b_1\} = \{b_1, l, v, b_2\} \\ Q_{b2} = Nb(b_2) \cup \{b_2\} = \{b_1, b_2, b_3, v\} \\ Q_{b3} = Nb(b_3) \cup \{b_3\} = \{b_3, b_2, v, r\} \end{cases} \tag{4}$$

We find that $Q_{b2} = P_v$. Thus, both $b_2$ and $v$ are the candidate points with multi-voxel width. Which one should be removed is based on their DFB-distances. It is noticed that $DFB(b_2) < DFB(v)$; thus, voxel $v$ is closer to the center of the blood vessel than $b_2$ is. According to the criterion, point $b_2$ is redundant and

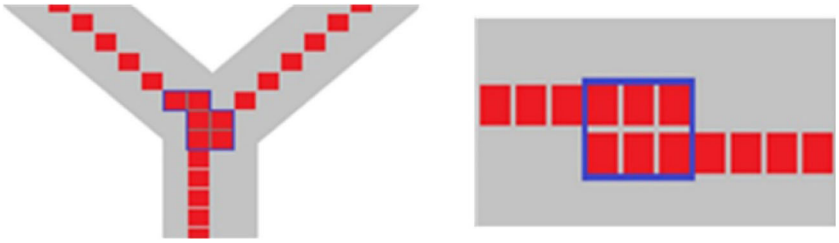


**Fig. 3** Diagram of centerline points with multi-voxel width in two cases. **a** At the bifurcation. **b** After multiple information fusion. The points in blue frame have multi-voxel width (Color figure online)

should be removed. We give the flowchart of the monocentric processing of centerline in Fig. 5, where the readers can find the implementation details.

After the monocentric processing of centerline, multi-voxel width still exists on certain centerline points. Hence, the monocentric processing can be implemented repeatedly until all the centerline points having single voxel width.

In summary, algorithm 1 gives the pseudo-code of the proposed monocentric centerline extraction method for ring-like blood vessels.

**Algorithm 1** A monocentric centerline extraction method for ring-like blood vessels

**Input:** Blood vessel data

**1: Selection of the original centerlines**

Sprinkle random points, and determine the $R$ seed points.

Generate $R$ original centerlines.

**2: Multiple information fusion**

Referring to Eq. (1), combine $R$ original centerlines and get a merged centerline.

Referring to Eq. (2), incorporate the neighbor points whose DFB-distances are larger than the current one.

**3: Monocentric processing of the centerline**

**for** $k_i = 1$ to $K$ (where $K$ is the number of iterations of the monocentric processing)

**for** $l_i = 1$ to $L_c$ (where $L_c$ is the number of centerline points)

$v$ is assigned as the $l_i^{\text{th}}$ centerline point.

Calculate $B$, $P_v$, $Q_{bi}$.

**if** $Q_{bi} \subset P_v$

$b_i$ should be removed

**elseif** $Q_{bi} = P_v$

Remove the centerline points with smaller DFB-distance value.

**end**

**end**

**end**

**Output:** Centerline of blood vessel

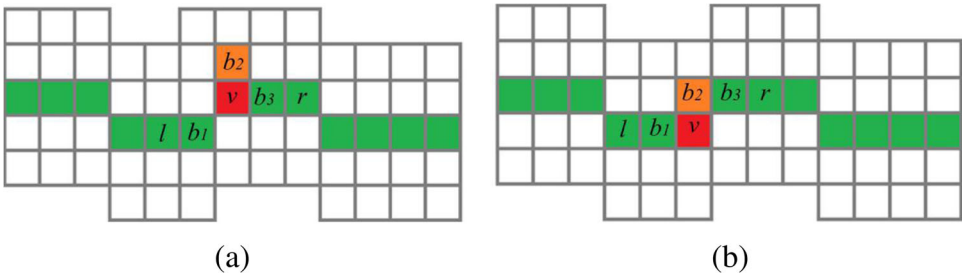


**Fig. 4** Diagram of monocentric processing of centerline. **a** $Q_{b2} \subset P_v$. **b** $Q_{b2} = P_v$. The red box is the current point and the orange box is the redundant point (Color figure online)

## 3 Results

### 3.1 Analysis methodology

The experiments were conducted on five groups of data to verify the feasibility of the proposed method. The synthetic dataset includes four groups of data. Data1 and data2 are simple simulated data that is generated from the ground truth centerlines (Fig. 6). Data3 and data4 are from a group of synthesized vascular datasets [11]. The group of data consists of 12 vasculatures, whose networks are substantially more and more complex. We chose two data from the group of synthesized vascular datasets and modified them by adding ring-like blood vessels as our experimental data (i.e., data3 and data4) in order to evaluate our proposed method (Fig. 7). Data5 is from the Designed Database of MR Brain Images of Healthy

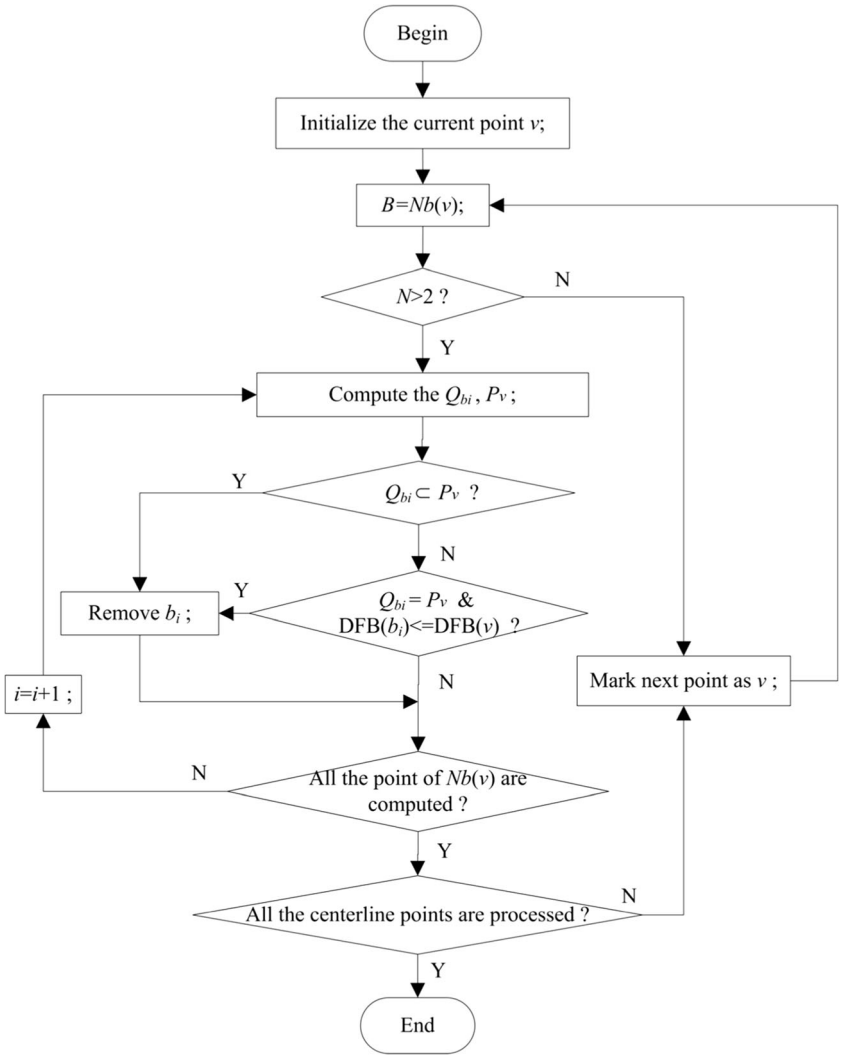


**Fig. 5** Flowchart of the monocentric processing of centerline

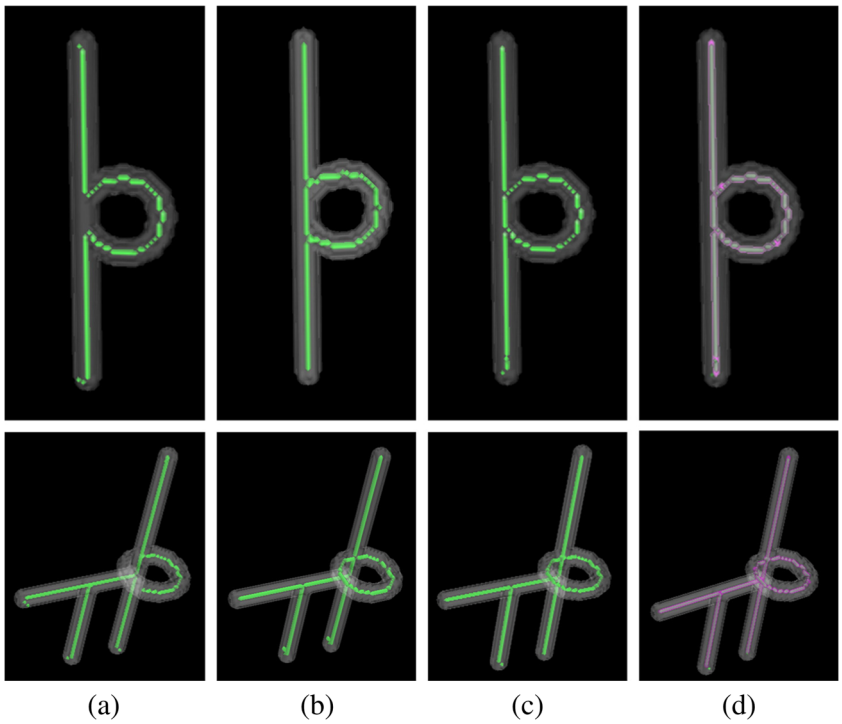


**Fig. 6** Results of centerline extraction on two simple simulation data. **a** Results of Wan et al.'s method. **b** Results of topological thinning. **c** Results of the proposed method. **d** Superposition results of the proposed method and the ground truth

Volunteers [5]. This database includes more than 100 human brain magnetic resonance angiography (MRA) images, in which 20 patients are scanned from which age range (18–29, 30–39, 40–49, 50–59, and 60+). Each group is equally divided by sex, diabetes history, hypertension, head trauma, psychiatric disease, or other symptoms or history likely to affect the brain. It is reported that the ring-like blood vessel often appears in the human brain, which is manifested in CoW. Thus we selected the data that have complete CoW to carry out the real data experimental verification (Fig. 8). The size of the data is $512 \times 512 \times 148$.

Wan et al.'s method [36] and the topological thinning [27] are the most commonly used centerline extraction methods in the area of topological description, virtual endoscope, and surgical planning. On the other hand, the topological thinning is more likely to extract a complete circular centerline since it equally treats the tree-like and ring-like blood vessels. Therefore, we compared our proposed method with these two methods to verify the feasibility from the perspective of quantitation and visual inspection. To quantitatively analyze the propose method, we employed three estimation criteria, namely average distance, modified Dice coefficient, and non-singularized count.

**Average distance** This is used to evaluate the displacement of the extracted centerline to the ground truth, representing the average minimum distance from each voxel on the ground truth to the voxel that on the centerline of our method. The

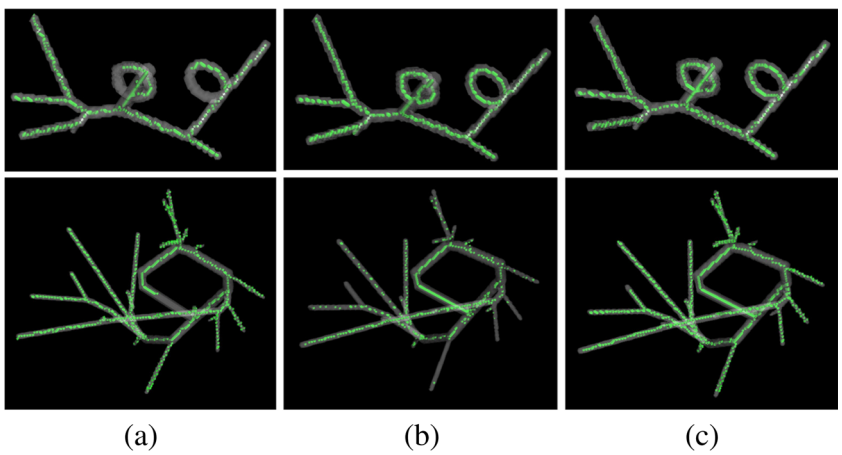


**Fig. 7** Results of centerline extraction on synthesized vascular datasets. **a** Results of Wan et al.'s method. **b** Results of topological thinning. **c** Results of the proposed method

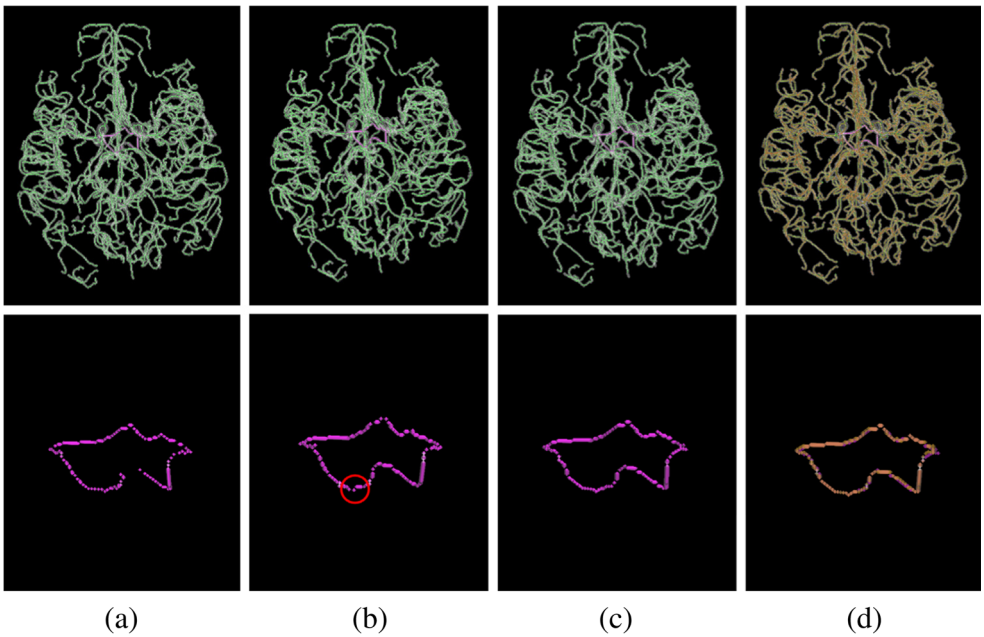


**Fig. 8** Results of centerline extraction on the Database of MR Brain Images. **a** Centerline extracted by Wan et al.'s method. **b** Centerline extracted by topological thinning. **c** Centerline extracted by the proposed method. **d** Superposition results of the proposed method (purple) and the ground truth (yellow) (Color figure online)

evaluation of average distance (*AD*) is based on Euclidean distance whose unit is pixel.

$$AD = \frac{\sum_{i=1}^{M_c} \min(dis(i))}{N_a} \tag{5}$$

where $N_a$ is the number of voxels on the ground truth centerline $C^t$, $M_c$ is the number of voxels on the centerline $C^p$ extracted by the proposed method, and $dis(i)$ is the distance from one voxel on $C^p$ to all the voxels on $C^t$.

**Modified Dice coefficient** This indicator is used to measure the overlap between the result of the proposed method and that of the ground truth. Because the centerline of blood vessel is sparse and thin compared with regional object, such as lung and liver, we modified the denominator of traditional Dice coefficient to the number of voxels on the ground truth centerline $C^t$. Thus, the modified Dice coefficient is calculated as the ratio of the number of correct voxels to the total voxel number on ground truth centerline.

$$MDC = \frac{C^t \cap C^p}{N_a} \tag{6}$$

where $C^t \cap C^p$ represents the number of overlapping voxels between $C^t$ and $C^p$, and $N_a$ is the number of voxels on the ground truth centerline $C^t$. The range of modified Dice coefficient (*MDC*) is within the interval [0, 1], where 0 stands for no overlapping, and 1 stands for completely overlapping between $C^t$ and $C^p$.

**Non-singularized count** Both *AD* and *MDC* characterize the accuracy of the extracted centerline from the overall quantitative point of view, which means they cannot quantify the extracted centerline in terms of single-voxel width or multi-voxel width. In order to quantitatively analyze the single-voxel width properties of the proposed method, we define the non-singularized count (*NSC*) as the count of centerline points with multi-voxel width as follows

$$NSC = count(centerline\ points\ with\ multi\text{-}voxel\ width) \tag{7}$$

The critical issue for the computation of *NSC* to accurately locate and count all the centerline points with multi-voxel width. We located the multi-voxel width points by using the same method as in monocentric processing. In other words, we judged whether the set composed by one centerline point and its neighbors is within the set of another centerline point and its neighbors. If the answer is yes, we located the current centerline point as the one with multi-voxel width. We refer the readers to Sect. 2.3 for a more detailed description for distinguishing multi-voxel width points.

### 3.2 Synthetic dataset

We first extracted the centerline by using the proposed method, Wan et al.'s method and topological thinning on the simple simulation data, whose results are given in Fig. 6. There are obvious absences of centerline points at the circle location of centerline using Wan et al.'s method (Fig. 6a). This is because that the centerline grows from a seed voxel along one side of the ring-like blood vessel, and the end point of this centerline does not link to the seed point. The results of using topological thinning are acceptable on the data1 which is quite smooth and

standardized, but it deviates from the centerline at the end point on data2 (Fig. 6b). Using the proposed method, we finely extracted the centerline on circle location and finally obtained a complete centerline (Fig. 6c), where the notch is repaired completely. Moreover, the extracted centerline by the proposed method is almost fully overlapped with the ground truth (Fig. 6d).

We further quantitatively evaluated the proposed method by using the three criteria (Table 1). Because the random seed sprinkling is involved in both the Wan et al.'s method and the proposed method, the quantitative results of these two methods are obtained by running five times on each data and then averaging them. The *AD* value of the proposed method is $0.0265 \pm 0.0085$ on data1, which is much smaller than that of Wan et al.'s method ($0.1693 \pm 0.0596$) and topological thinning (0.1600). And the *MDC* of our proposed method is comparable with these two contrast methods. The lower *AD* and higher *MDC* demonstrates the accuracy of the proposed centerline extraction method. In addition, the *NSC* values of the proposed method and topological thinning are always zero, which means that the proposed method has detected all the multi-voxel width points and has removed it. Because the simulation data are relatively simple, the phenomenon of multi-voxel width on centerline extracted by these two contrast methods is not serious.

Although experiments on two groups of simple simulation data verify the feasibility of the proposed method to a certain extent, the simulation data are quite smooth and standardized. Therefore, we employed two synthesized vascular data (i.e., data3 and data4) to test the performance of the proposed method on complex synthesized blood vessels. The two synthesized vascular data have no ground truth centerlines, so the results can only be evaluated through visual inspection. The results of three different methods are shown in Fig. 7. It is noticed that there are lots of notches on the centerlines extracted by Wan et al.'s method (Fig. 7a). The topological method performs well on data3 which is neat and uniform. However, the extracted centerline is broken when the vascular radius is quite small or changes dramatically (Fig. 7b). In contrary, the proposed method properly restores the missing centerlines at notch positions (Fig. 7c), as well as obtains a continuous centerline. Furthermore, the *NSC* values of data3 and data4 by using Wan et al.'s method are $4.8 \pm 0.8367$ and $10.6 \pm 1.5166$, respectively (Table 2), and those by using topological thinning are 3 and 10, respectively. The *NSC* values on both data3 and data4 employing our proposed method are reduced to zeros. It fully guarantees that the extracted centerline has only single voxel width, which can facilitate the accurate follow-up diagnosis and planning of vascular related diseases.

### 3.3 Real MRA dataset

After evaluation on the synthetic data, it is necessary to examine the performance of the proposed method on more complex clinical vascular networks. Thus, we test the feasibility of the proposed method on cerebral blood vessels obtained from the Designed Database of MR Brain Images of Healthy Volunteers that contain complete circle of Willis (CoW). Compared with the simple and synthesized data, the cerebral MRA data have the characteristics of irregularity and high complexity. The centerlines extracted by the proposed method and these two contrast methods are shown in Fig. 8.

Due to the existence of many broken cerebral blood vessels in the brain data, we have to randomly sprinkle millions of points on the volumetric data to guarantee that every original centerline is extracted from all the blood vessels. The extracted centerlines using Wan et al.'s method and topological thinning are given in Fig. 8a, b, respectively, where we highlight the CoW at the bottom insets. On one hand, the Wan et al.'s method fails on the ring-like CoW, although it almost successfully extracts the centerlines of all the tree-like cerebral blood vessels. On the other hand, the extracted centerlines by topological thinning are discontinuous in many parts no matter on the tree-like cerebral vessels or on the ring-like CoW. In contrary, the proposed method obtains intact centerlines on the CoW and other tree-like blood vessels (Fig. 8c). Furthermore, the centerlines extracted by the proposed method nearly completely overlap with the ground truth (Fig. 8d).

**Table 1** Results of quantitative analysis on data1 and data2

| | | *AD* | | *MDC* | | *NSC* | |
|---|---|---|---|---|---|---|---|
| | | Mean (pixel) | Std (pixel) | Mean (%) | Std (%) | Mean (pixel) | Std (pixel) |
| Data1 | Wan et al.'s method | 0.1693 | 0. 0596 | 94.42 | 2.43 | 1.4 | 0.5477 |
| | Topological thinning | 0.1600 | – | 97.36 | – | 0 | – |
| | Proposed method | *0.0265* | 0.0085 | *98.37* | 1.12 | *0* | 0 |
| Data2 | Wan et al.'s method | 0.5717 | 0.0756 | 91.48 | 0.55 | 2.8 | 0.8165 |
| | Topological thinning | 0.0464 | – | 97.84 | – | 0 | – |
| | Proposed method | *0.0335* | 0.0059 | *98.90* | 0.89 | *0* | 0 |

The italic entries are the results of proposed method

**Table 2** Results of quantitative analysis on data3 and data4

| | | *NSC* | |
|---|---|---|---|
| | | Mean (pixel) | Std (pixel) |
| Data3 | Wan et al.'s method | 4.8 | 0.8367 |
| | Topological thinning | 3 | – |
| | Proposed method | *0* | 0 |
| Data4 | Wan et al.'s method | 10.6 | 1.5166 |
| | Topological thinning | 10 | – |
| | Proposed method | *0* | 0 |

The italic entries are the results of proposed method

The results of quantitative analysis for the proposed method and these two compared methods are given in Table 3. The lower *AD* (0.4804 ± 0.0061) and acceptable high *MSD* (0.9910 ± 0.0020) demonstrate that the extracted centerline by our proposed method is closer to the ground truth. In addition, the proposed method can also fully remove the centerline points of multi-voxel width supported by the *NSC* value is always zero. It is noticed that the *MSD* of topological thinning is slightly higher than that of the proposed method. This is because nearly all the points on the ground truth centerline can find the overlapped points on the extracted centerline using topological thinning, which has serious multi-voxel width problem (whose *NSC* is 336). In this regard, the quantitative analysis further demonstrates that the proposed method outperforms Wan et al.'s method and topological thinning on clinical cerebral blood vessels.

## 4 Discussion

To repair the notches of the extracted centerlines on ring-like blood vessels, we employed two types of information, i.e., the information of multiple original centerlines and local maximum DFB-distances. Because the complementary information exists in the original centerlines, we can obtain a merged centerline without notches only if we acquire as many original centerlines as possible. As a matter of fact, no more than three original centerlines are enough for the proposed method to form a complete merger centerline. The incorporation of neighbor points with higher DFB values into the merged centerline is under the consideration of accuracy. There are lots of off-centerline points at the notch positions and end points (root and leaves). Thus, we have to incorporate the points who are closer to the vascular center, which is the basis of extracting an accurate centerline after monocentric processing.

The multi-voxel width of original centerlines commonly occurs on vascular branch or on the blood vessel whose radii change dramatically. The reason behind this is that the Euclidean distances from either pixels of the centerline to the boundary pixels sometimes are the same [41]. Moreover, another reason is the information fusion of multiple original centerlines and the local maximum of DFB-distances. Thus, we singularize the centerline by employing the proposed monocentric processing, whose input is the merged centerline formed by Eqs. (1) and (2). Based on the topology of the merged centerline, we gradually remove the points with multi-voxel width by judging if the set composed by one centerline point and its neighbors is within the set of another centerline point and its neighbors. This strategy not only eliminated all the multi-voxel width centerline points but also guaranteed the connectivity of the centerline.

Theoretically, the proposed monocentric processing seems like topological thinning methods [3, 6, 8, 25, 33]. However, the topological thinning performs well only on simple simulation data with a fixed scale (Fig. 6). They fail to extract the entire centerlines no matter on synthesized vascular data or on the MR brain image (Figs. 7 and 8), due to the complex vascular networks with multiple scales. Moreover, the monocentric processing is more efficient compared with topological thinning method, because we only handle the merged centerline points rather than the entire blood vessel.

## 5 Conclusions

In conclusion, we proposed a monocentric centerline extraction method aiming to solve the failure of centerline extraction on ring-like blood vessels and the problem of centerline points with multi-voxel width. The proposed method mainly consists

**Table 3** Results of quantitative analysis on data5

| | | *AD* | | *MDC* | | *NSC* | |
|---|---|---|---|---|---|---|---|
| | | Mean (pixel) | Std (pixel) | Mean (%) | Std (%) | Mean (pixel) | Std (pixel) |
| Data5 | Wan et al.'s method | 0.5583 | 0. 0670 | 96.99 | 0.0062 | 55.8 | 0.0152 |
| | Topological thinning | 0.5042 | – | 99.45 | – | 336 | – |
| | Proposed method | *0.4804* | 0.0061 | *99.10* | 0.0020 | *0* | 0 |

The italic entries are the results of proposed method

of multiple information fusion and monocentric processing. The performance is tested on simple simulation data, synthesized blood vessels, and clinical cerebral blood vessels. Compared with previous methods, the proposed method can properly complete the centerline extraction on ring-like blood vessel and eliminate the points with multi-voxel width as well. The proposed centerline extraction method is of great importance for the clinical and preclinical quantitative analysis of vascular related diseases.

**Acknowledgements** This work was partly supported by the National Natural Science Foundation of China under Grant Nos. 61601363, 61372046, 61401264, 11571012, 61640418, 81530058, and 61601154; the National Key R&D Program of China under Grant No. 2016YFC1300300; the Science and Technology Plan Program in Shaanxi Province of China under Grant Nos. 2013K12-20-12 and 2015KW-002; the Natural Science Research Plan Program in Shaanxi Province of China under Grant Nos. 2017JQ6017, 2015JM6322, and 2015JZ019; and the Scientific Research Foundation of Northwest University. The MR brain images from healthy volunteers used in this paper were collected and made available by the CASILab at The University of North Carolina at Chapel Hill and were distributed by the MIDAS Data Server at Kitware, Inc.

**Compliance with ethical standards**

**Conflict of interest** The authors declare that they have no conflict of interest.

**Ethical approval** All the MR brain data are obtained from public database. No human/animal experiments are involved in this paper.

## References

1. Antiga L (2002) Patient-specific modeling of geometry and blood flow in large arteries. PhD Dissertation. Politecnico di Milano
2. Aylward S, Pizer S, Eberly D, Bullitt E (1996) Intensity ridge and widths for tubular object segmentation and description. In: Anon (ed) Proceedings of the workship on mathematical methods in biomedical image analysis. IEEE, San Francisco, CA, pp 131–138
3. Bian Z, Tan W, Yang J, Liu J, Zhao D (2014) Accurate airway centerline extraction based on topological thinning using graph-theoretic analysis. Biomed Mater Eng 24:3239–3249
4. Bitter I, Kaufman AE, Sato M (2001) Penalized-distance volumetric skeleton algorithm. IEEE Trans Vis Comput Graph 7:195–206
5. Bullitt E, Zeng DL, Gerig G, Aylward S, Joshi S, Smith JK, Lin WL, Ewend MG (2005) Vessel tortuosity and brain tumor malignancy: a blinded study. Acad Radiol 12:1232–1240. https://doi.org/10.1016/j.acra.2005.05.027
6. A C, D B GS (1985) A width-independent fast thinning algorithm. IEEE Trans Pattern Anal Mach Intell 7:463–474
7. Ćurić G (2014) Function of circle of Willis. J Cereb Blood Flow Metab 34:578–584
8. Ding M, Tong R, Liao SH, Dong J (2009) An extension to 3D topological thinning method based on LUT for colon centerline extraction. Comput Methods Prog in Biomed 94:39–47
9. Elattar MA, Wiegerinck EM, Planken RN, Vanbavel E, van Assen HC, Baan J Jr, Marquering HA (2014) Automatic segmentation of the aortic root in CT angiography of candidate patients for transcatheter aortic valve implantation. Med Biol Eng Comput 52:611–618. https://doi.org/10.1007/s11517-014-1165-7
10. Gray-Edwards HL, Salibi N, Josephson EM, Hudson JA, Cox NR, Randle AN, McCurdy VJ, Bradbury AM, Wilson DU, Beyers RJ et al (2014) High resolution MRI anatomy of the cat brain at 3 Tesla. J Neurosci Methods 227:10–17. https://doi.org/10.1016/j.jneumeth.2014.01.035
11. Hamarneh G, Jassi P (2010) VascuSynth: simulating vascular trees for generating volumetric image data with ground-truth segmentation and tree analysis. Comput Med Imaging Graph 34:605–616. https://doi.org/10.1016/j.compmedimag.2010.06.002
12. Hassouna MS, Farag AA (2005) Robust centerline extraction framework using level sets. IEEE Comput Soc Conf Comput Vis Pattern Recog 1: 458–465
13. Heinzer S, Krucker T, Stampanoni M, Abela R, Meyer EP, Schuler A, Schneider P, Mueller R (2006) Hierarchical microimaging for multiscale analysis of large vascular networks. NeuroImage 32:626–636. https://doi.org/10.1016/j.neuroimage.2006.03.043
14. Heinzer S, Kuhn G, Krucker T, Meyer E, Ulmann-Schuler A, Stampanoni M, Gassmann M, Marti HH, Mueller R, Vogel J (2008) Novel three-dimensional analysis tool for vascular trees indicates complete micro-networks, not single capillaries, as the angiogenic endpoint in mice overexpressing human VEGF(165) in the brain. NeuroImage 39:1549–1558. https://doi.org/10.1016/j.neuroimage.2007.10.054
15. Hernández-Hoyos M, Orkisz M, Puech P, Mansard-Desbleds C, Douek P, Magnin IE (2002) Computer-assisted analysis of three-dimensional MR angiograms. Radiographics Rev Publ Radiol Soc North Am Inc 22:421–436
16. Huang A, Liu HM, Liu HM, Lee CW, Yang CY, Tsang YM, Tsang YM (2009) On concise 3-D simple point characterizations: a marching cubes paradigm. IEEE Trans Med Imaging 28:43–51
17. Jasika N, Alispahic N, Elma A, Ilvana K, Elma L, Nosovic N (2012) Dijkstra's shortest path algorithm serial and parallel execution performance analysis. 2012 Proc 35th Int Convention MIPRO 2012: 1811-1815
18. Jin D, Iyer KS, Chen C, Hoffman EA, Saha PK (2016) A robust and efficient curve skeletonization algorithm for tree-like objects using minimum cost paths. Pattern Recognition Letters 76:32–40. https://doi.org/10.1016/j.patrec.2015.04.002
19. Kang DG, Suh DC, Ra JB (2009) Three-dimensional blood vessel quantification via centerline deformation. IEEE Trans Med Imaging 28:405–414
20. Krissian K, Malandain G, Ayache N (1998) Model based multiscale detection and reconstruction of 3D vessels. HAL - INRIA: RR-3442
21. Krissian K, Malandain G, Ayache N (1998) Model based multiscale detection and reconstruction of 3D vessels. INRIA, City
22. Kumar RP (2013) Study on liver blood vessel movement during breathing cycle. Colour Vis Comput Symp 8255:1–5
23. Kumar RP, Albregtsen F, Reimers M, Edwin B, Lango T, Elle OJ (2015) Three-dimensional blood vessel segmentation and centerline extraction based on two-dimensional cross-section analysis. Ann Biomed Eng 43:1223–1234. https://doi.org/10.1007/s10439-014-1184-4
24. Lahousse L, Tiemeier H, Ikram MA, Brusselle GG (2015) Chronic obstructive pulmonary disease and cerebrovascular disease: a comprehensive review. Respir Med 109:1371–1380. https://doi.org/10.1016/j.rmed.2015.07.014
25. Lam L, Lee SW, Suen CY (1992) Thinning methodologies—a comprehensive survey. IEEE Trans Pattern Anal Mach Intell 14:869–885
26. Lee J, Kim G, Lee H, Shin BS, Shin YG (2008) Fast path planning in virtual colonoscopy. Comput Biol Med 38:1012–1023
27. Lee TC, Kashyap RL, Chu CN (1994) Building skeleton models via 3-D medial surface/axis thinning algorithms. Cvgip Graph Model Image Process 56:462–478

28. Li H, Yezzi A (2007) Vessels as 4-D curves: global minimal 4-D paths to extract 3-D tubular surfaces and centerlines. IEEE Trans Med Imaging 26:1213–1223. https://doi.org/10.1109/tmi.2007.903696
29. Mendonça AM, Campilho A (2006) Segmentation of retinal blood vessels by combining the detection of centerlines and morphological reconstruction. IEEE Trans Med Imaging 25:1200–1213
30. Mortier P, De Beule M, Van Loo D, Masschaele B, Verdonck P, Verhegghe B (2008) Automated generation of a finite element stent model. Med Biol Eng Comput 46:1169–1173. https://doi.org/10.1007/s11517-008-0410-3
31. Pagidipati NJ, Gaziano TA (2013) Estimating deaths from cardiovascular disease: a review of global methodologies of mortality measurement. Circulation 127:749–756. https://doi.org/10.1161/circulationaha.112.128413
32. A SR, B E (2002) Initialization, noise, singularities, and scale in height ridge traversal for tubular object centerline extraction. IEEE Trans Med Imaging 21:61–75
33. Sadleir R, Whelan PF (2005) Colon centerline calculation for CT colonography using optimised 3D topological thinning. Comput Med Imaging Graph 29:251–258
34. Serrador JM, Picot PA, Rutt BK, Shoemaker JK, Bondar RL (2000) MRI measures of middle cerebral artery diameter in conscious humans during simulated orthostasis. Stroke 31:1672–1678
35. Tillich M, Hill BB, Paik DS, Petz K, Napel S, Zarins CK, Rubin GD (2001) Prediction of aortoiliac stent-graft length: comparison of measurement methods. Radiology 220:475–483
36. Wan M, Liang Z, Ke Q, Hong L, Bitter I, Kaufman AE (2002) Automatic centerline extraction for virtual colonoscopy. IEEE Trans Med Imaging 21:1450–1460
37. Xin L, Gao Z, Xiong H, Ghista D, Ren L, Zhang H, Wu W, Huang W, Hau WK (2016) Three-dimensional hemodynamics analysis of the circle of Willis in the patient-specific nonintegral arterial structures. Biomech Model Mechanobiol 15:1–18
38. XuJ, Feng D, Wu J, Cui Z (2009) Robust centerline extraction for tree-like blood vessels based on the region growing algorithm and level-set method. 2009 Sixth Int Conf Fuzzy Syst Knowl Discov 4:586–591 Doi https://doi.org/10.1109/FSKD.2009.916
39. Yang G, Kitslaar P, Frenay M, Broersen A, Boogers MJ, Bax JJ, Reiber JHC, Dijkstra J (2012) Automatic centerline extraction of coronary arteries in coronary computed tomographic angiography. Int J Cardiovasc Imaging 28:921–933
40. Zhao F, Liang J, Chen D, Wang C, Yang X, Chen X, Cao F (2015) Automatic segmentation method for bone and blood vessel in murine hindlimb. Med Phys 42:4043–4054. https://doi.org/10.1118/1.4922200
41. Zhao F, Liang J, Chen X, Liu J, Chen D, Yang X, Tian J (2016) Quantitative analysis of vascular parameters for amicro-CT imaging of vascular networks with multi-resolution. Med Biol Eng Comput 54:511–524. https://doi.org/10.1007/s11517-015-1337-0
42. Zhao F, Liu J, Qu X, Xu X, Chen X, Yang X, Cao F, Liang J, Tian J (2014) In vivo quantitative evaluation of vascular parameters for angiogenesis based on sparse principal component analysis and aggregated boosted trees. Phys Med Biol 59:7777–7791

**Fengjun Zhao** received the Ph.D degree in Signal and Information Processing from Xidian University in 2015. He is now a lecturer in Northwest University, focusing on medical image processing.

**Feifei Sun** received the BEng degree in Electronic Information Engineering from Zhongyuan University of Technology. She is now a master in Signal and Information Processing from Northwest University.

**Yuqing Hou** received the MEng Degrees from Northwest University and Doshisha University respectively. She is now a professor from Northwest University and has directed many research projects.

**Yanrong Chen** received the BEng degree in Internet of Things Engineering from Central South University. She is now a Ph.D student in Northwest University and concentrates on image segmentation.

**Dongmei Chen** received the Ph.D degree from Xidian University in 2015. She is a lecturer in Hangzhou Dianzi University and interested in the reconstruction of X-ray luminescence computed tomography.

**Xin Cao** received the Ph.D degree from Xidian University in 2016. He is now a lecturer in Northwest University and devoted to the preclinical research of Cerenkov imaging and its applications.

**Huangjian Yi** received the Ph.D degree from Xidian University in 2013. She is now a lecturer from Northwest University, whose research interests are the algorithms for fluorescent molecular imaging.

**Bin Wang** received the MEng degree from Northwest University. He is now a lecturer from Northwest University and interested in image mapping and registration between multi-modality imaging.

**Xiaowei He** received the Ph.D degree from Xidian University in 2011. He is now a professor and deputy dean of the graduate school in Northwest University, focusing on multi-modality molecular imaging.

**Jimin Liang** received the Ph.D degree from Xidian University in 2000. He is now a professor in Xidian University, who is skilled in medical imaging and has published more than 50 journal papers.